PERGAMON

PII: S1359-6454(99)00189-5

Acta mater. Vol. 47, No. 11, pp. 3181–3187, 1999
Published by Elsevier Science Ltd
On behalf of Acta Metallurgica Inc.
Printed in Great Britain
1359-6454/99 $20.00 + 0.00

KINETIC PHASE FIELD PARAMETERS FOR THE Cu–Ni SYSTEM DERIVED FROM ATOMISTIC COMPUTATIONS

J. J. HOYT[1]†, B. SADIGH[2], M. ASTA[1] and S. M. FOILES[1]

[1]Computational Materials Science Department, Sandia National Laboratories, Livermore, CA 94550, U.S.A. and [2]Lawrence Livermore National Laboratories, Livermore, CA 94550, U.S.A.

(Received 19 February 1999; accepted 1 June 1999)

Abstract—In the phase field model of binary solidification the mobility terms which appear in the governing rate equations can be estimated from the liquid diffusion coefficients of the pure elements and the velocity of the solid–liquid interface as a function of undercooling. Molecular dynamics simulations utilizing embedded atom potentials have been employed to compute the liquid diffusivities for pure Cu and Ni in the vicinity of their melting points. In both cases the diffusion coefficient is found to vary linearly with temperature and the results are in good agreement with experimental values which are available for Cu. The simulations were also employed to obtain the boundary velocities in three different low index growth directions. The results for Cu and Ni were found to be very similar, with the slope of the velocity–undercooling curve at small undercoolings varying in the range 45–18 cm/s/K. Anisotropy in the growth behavior was observed with $V_{100} > V_{110} > V_{111}$. The solid–liquid interface velocities were found to be a factor of 4–5 less than the theoretical upper limit derived previously. *Published by Elsevier Science Ltd on behalf of Acta Metallurgica Inc.*

Keywords: Solidification; Copper; Nickel; Theory and modeling (kinetics, transport, diffusion)

1. INTRODUCTION

The advantages of the phase field model of solidification are now well established. By defining a continuous variable, that is the phase field, which defines the state of the system, liquid or solid, at each point, one circumvents the difficult numerical task of tracking a sharp solid–liquid boundary. Furthermore, the partial differential equations arising in the phase field formulation are able to describe quite naturally the coalescence of two distinct solid regions, a problem which leads to mathematical singularities in the alternative sharp interface description. To date, numerous studies have examined various mathematical aspects of the phase field method including: asymptotic analyses which rigorously demonstrate the equivalence of phase field models and the sharp interface description in the limit of small interface widths [1–3], extending the phase field ideas to include more complicated phenomena such as nucleation [4, 5], implementing the general phase field framework to model solid–solid transformations such as particle coarsening [6, 7] and grain growth [8, 9], and developing very efficient numerical algorithms [10–12]. On the other hand, very few studies have attempted to apply the phase field model to actual alloy systems. The reason for the lack of detailed comparisons between theory and experiment stems from the fact that several parameters which appear in the kinetic equations—mobilities, free energies, interfacial energies, etc.—are unknown for most alloys. In an important contribution, Wheeler *et al.* [13] showed that, for systems whose free energy vs composition can be considered ideal, all necessary input parameters of the phase field model of solidification can be derived from a knowledge of the liquid diffusion coefficients, the solid–liquid interfacial free energies and the velocities of the solid–liquid interface as a function of undercooling, where the parameters are required for both of the pure components in the alloy. The authors provided estimates of these six parameters for the Cu–Ni system and the model was subsequently utilized by Warren and Boettinger [14] to study dendrite formation and microsegregation patterns. Although the required materials properties can, in principle, be obtained from experiment, in practice the measurements are very difficult if not impossible to perform. Therefore, it is the purpose of this work to demonstrate how atomistic simulations can be utilized to obtain kinetic parameters of the phase field model (the surface free energy calculations will be described in a forthcoming publication).

The embedded atom method (EAM) is a semi-empirical approach to the description of interatomic potentials which extends beyond simple pair interactions. The EAM has been employed in numerous studies of thermodynamic, defect and mechanical properties of several alloy systems [15]. Despite the

†To whom all correspondence should be addressed.

fact that EAM potentials are generated from a fit to measured properties of the solid, Foiles demonstrated that the technique predicts very well the structure [16] and thermodynamic properties [17] of liquids. In more recent work Alemany *et al.* [18, 19] employed the EAM with molecular dynamics (MD) simulations to compute the diffusivity of several transition metal liquids. Asta *et al.* [20] examined structural, thermodynamic and transport properties of liquid Ni–Al alloys using both Monte Carlo and MD techniques in conjunction with EAM potentials. Rodriguez de la Fuente and Soler [21] used the EAM to examine the structure of amorphous Ni following an MD quench from the liquid state. The EAM-MD approach will be used in the present study to compute the diffusion coefficient vs temperature of pure Ni and Cu in the vicinity of their melting points and to calculate the velocity of the 100, 110 and 111 solid–liquid interfaces as a function of undercooling. For all of the simulations, we have employed the EAM potential originally developed by Foiles *et al.* [22]; however, the aforementioned work of Alemany *et al.*, which used the Voter–Chen potential [23], will serve as a basis for comparison. In addition, an *ab initio* MD simulation has been performed by Pasquarello *et al.* [24] in which the diffusion coefficient of liquid Cu was reported at 1500 K. The first principles result will be used to test the reliability of the empirical EAM approach. Throughout the study the atomistic simulation results will be compared with available experimental data where possible.

2. NUMERICAL SIMULATION PROCEDURES

The molecular dynamics algorithm employed in this study has been used successfully in the past to study various dynamic properties of both liquid and solid alloys [15]. For the diffusion measurements a periodic cell of dimension $6 \times 6 \times 6$ f.c.c. unit cells (864 atoms) was melted at 2500 K and subsequently equilibrated at the temperature of interest and zero pressure. The system size employed in the present work is larger than the diffusion study of Alemany *et al.* and simulations performed on a much larger system (2048 atoms) resulted in no difference in the computed diffusivity. The equilibration step employed a time step of 5 fs for a total simulation time of 40 ps. Microcanonical (constant energy-volume-number) simulations were performed to collect velocity–velocity correlation data (see below) where the total time was 50 ps and the time step was 1 fs.

The solid–liquid interface velocity simulations were carried out in the following way. A lattice with $20 \times 8 \times 8$ unit cells (5120 atoms) and with the $\langle 100 \rangle$ directions coincident with the cartesian coordinates was generated. Test simulations on a larger size periodic cell (8000 atoms) indicated that there is no effect of system size on the measured interface velocity. Initially, all atoms located less than one quarter of the total length of the periodic cell were held fixed and the remainder of the system was melted as described above. Figure 1 shows an example of the starting configuration for the case of Ni in the 100 direction. Upon solidification the solid slab on the left of the figure will move into the liquid and because of the periodic boundary conditions, the solid will also move from right to left starting from the extreme right-hand end of the cell. The velocity of the atoms was then rescaled to some temperature below the melting point and an MD simulation was performed using a time step of 1 fs. During solidification the atoms on the left-hand side of the cell which were initially fixed in position were allowed to move. The simulation was terminated when complete solidification was achieved (about 40 ps). The above method measures

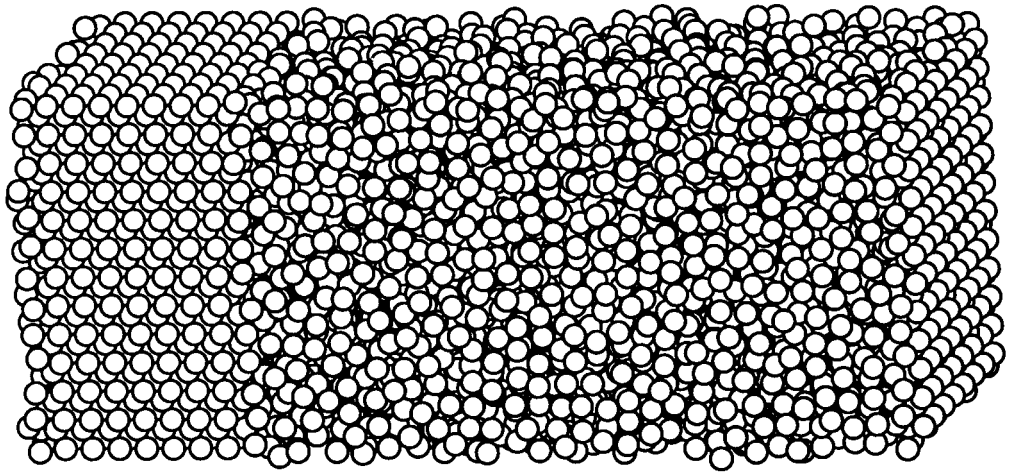

Fig. 1. The initial configuration of atoms used in the simulation of solid–liquid interface motion. The example shown is for 100 Ni at 1500 K.

the velocity of the 100 interface; two other interfaces were investigated, 110 and 111. For these interfaces the initial lattice was rotated such that the required crystal plane was oriented perpendicular to the long direction. Since 110 and 111 are more densely packed directions, more atoms were required to retain a total cell length approximately the same (80 Å) as in the 100 case. Thus 6144 atoms were employed for the 110 simulations and 6408 total atoms were necessary in the 111 case. It is important to note that during solidification latent heat is generated and therefore a constant energy–volume MD simulation is inappropriate. Rather, a constant temperature–pressure ensemble was utilized and the temperature was maintained constant using standard techniques [25]. It should be noted that the volume of the periodic cell was allowed to translate during the solidification process and thus there will be a contribution to the interface velocity arising from the difference in density between the solid and liquid. Since the density difference is on the order of 3–5%, this contribution is small.

3. RESULTS AND DISCUSSION

3.1. Diffusion coefficient

There are two methods for computing liquid diffusivities from MD simulations [26]. The first relates the diffusion coefficient to the long time behavior of the mean square displacement of an atom and is given by

$$D = \lim_{t\to\infty} \frac{1}{6t} \langle |\mathbf{r}(t) - \mathbf{r}(0)|^2 \rangle. \tag{1}$$

The position of an atom at any time t is denoted by $\mathbf{r}(t)$, D is the diffusion coefficient and the angular brackets indicate an average with respect to all atoms in the simulation and over all time origins. The second technique for computing D is through the formulation of the velocity–velocity correlation function, $Z(t)$, which is defined as

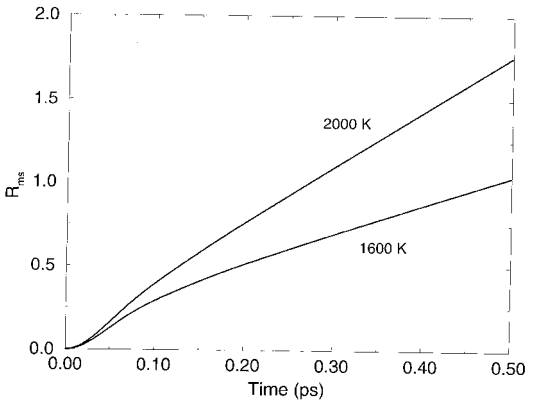

Fig. 2. Average r.m.s. displacement of Ni atoms as a function of time for two different temperatures. The slope of the lines at long times is proportional to the diffusion coefficient.

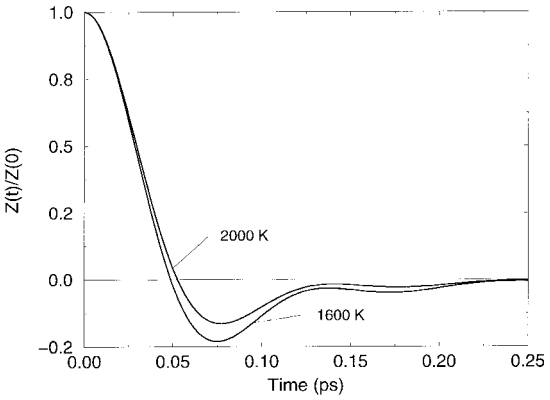

Fig. 3. The velocity–velocity correlation function normalized by its value at $t = 0$ vs time for 1600 and 2000 K. The integral of the curves over all time yields the diffusion coefficient.

$$Z(t) = \frac{1}{3} \langle \mathbf{u}(t) \cdot \mathbf{u}(0) \rangle \tag{2}$$

where $\mathbf{u}$ is the velocity vector. The diffusivity is related to the function $Z(t)$ by a straightforward integration over all time, that is

$$D = \int_0^\infty Z(t)\, \mathrm{d}t. \tag{3}$$

Figure 2 shows the mean square displacement, that is the term in angular brackets in equation (1), vs the time for liquid Ni at 1600 and 2000 K. After a short transient period of approximately 0.2 ps a linear relationship is established with a slope equal to $6D$. The increased diffusivity with increasing temperature is clearly observed. Figure 3 shows the velocity–velocity correlation function normalized by its value at $t = 0$ vs the time for Ni. The two temperatures shown are again 1600 and 2000 K. It can be seen that all velocity correlations decay rapidly and are essentially zero after about 0.5 ps. The negative correlation observed in the vicinity of the minimum at about 75 fs is a well-known effect in dense fluids and arises due to backscattering resulting from the cage of atoms which surrounds any given atom. As is also typical in fluid systems this so-called cage effect becomes less pronounced as the temperature is increased. The diffusion coefficient as determined by equation (1) at 2000 K was found to be $5.54 \times 10^{-5}\ \mathrm{cm}^2/\mathrm{s}$ whereas the diffusivity computed via the $Z(t)$ correlation function was $5.67 \times 10^{-5}\ \mathrm{cm}^2/\mathrm{s}$. The error of about 2.5% demonstrates the equivalence of the two methods.

Figure 4 plots the diffusion coefficient of Ni (filled squres) and Cu (filled circles) as a function of temperature. At moderate undercoolings and at the short time scales required for a diffusivity computation, there is no evidence in the MD simulations to indicate crystallization (for example, a drift in the average temperature in the system). Therefore, the diffusion data include three points in the undercooled regime and the range of the data is from

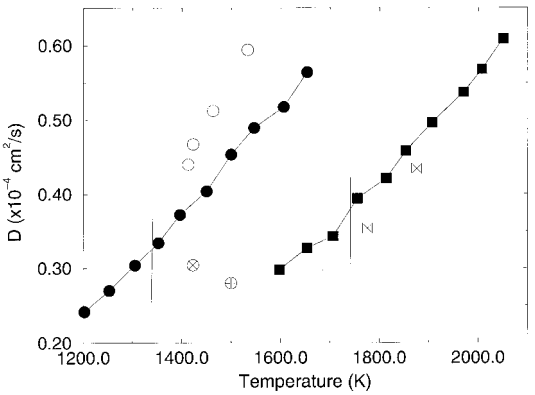

Fig. 4. The diffusion coefficient of pure Cu (filled circles) and Ni (filled squares) as a function of temperature. The vertical lines label the position of the EAM melting temperature. The symbols filled with a cross are the MD results of Alemany *et al.* [18, 19] and the open circles correspond to the experimental data of Henderson and Yang [28]. The symbol ⊕ is the *ab initio* calculation of Ref. [24]

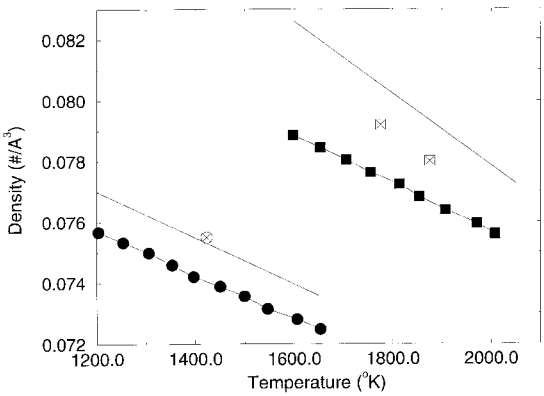

Fig. 5. Number density in the liquid phase computed with the EAM potentials as a function of temperature for Cu (filled circles) and Ni (filled squares). The solid lines correspond to experimental data [29] and the symbols filled with crosses denote the densities used in the simulations of Alemany *et al.* [18, 19].

140 K below the melting temperature to 310 K above T_m. The vertical lines on each curve indicate the EAM melting temperatures which are 1340 K for Cu and 1740 K for Ni [17]. Data for both Ni and Cu suggest a nearly linear dependence with temperature consistent with experimental data for several pure metals and are in agreement with phenomenological theories of liquid phase diffusion [27]. A linear regression analysis yields the following temperature behavior: $D_{Ni} = 6.92 \times 10^{-4}(T - T_M) + 0.382$ and $D_{Cu} = 7.219 \times 10^{-4}(T - T_M) + 0.332$ in units of 10^{-4} cm^2/s (Å^2/ps).

The symbols filled with crosses in Fig. 3 label the diffusion coefficients computed by Allemany *et al.* using the Voter–Chen (VC) EAM potential rather than the Foiles–Baskes–Daw potential. It should be pointed out however that a significant difference between the present computations and those of Alemany *et al.* is the fact that the previous study used the experimental value of the liquid density when performing the MD simulations. The filled symbols of Fig. 4 were obtained by equilibrating the liquids at each temperature (zero pressure) to obtain the EAM predicted density. The results for Ni are within fairly good agreement, the VC results being approximately 10–15% lower and the trend with temperature appears to be consistent. For Cu the agreement is somewhat worse, on the order of 20%, and the VC potential again yields a lower value. The open circles shown in Fig. 3 are results from the capillary reservoir techniques of Henderson and Yang [28]. Agreement between the present simulations and experiment is fairly good, particularly at the lower temperatures, with the EAM predicting consistently lower values. Because of the scatter in the experimental data it is difficult to confidently glean the behavior with temperature, but it appears that the simulations predict a somewhat smaller slope than the measurements. It is interesting to note that the Foiles–Baskes–Daw potential is in better agreement with experiment than the Voter–Chen results shown in Fig. 4. The improved agreement is surprising given that the Alemany *et al.* investigation fixed the number density of the liquid equal to the experimental value. The closer agreement between EAM and experiment is also surprising when one compares the results of an *ab initio* MD study [24] which is denoted by the symbol ⊕ in Fig. 4. The *ab initio* result, which is of course free of any inaccuracies associated with the assumption of an empirical potential, is in fact furthest removed from the experimental results.

An important quantity in many phenomenological theories of transport phenomena in liquids is the number density and thus it is of interest to compare the EAM computed density to the known experimental values. Figure 5 shows such a comparison where again the filled circles (squares) are the results for Cu (Ni). The experimental number density vs temperature behavior is shown as the solid line [29]. The agreement is excellent for Cu; the EAM values are consistently below experiment by just 2%. EAM results for Ni show a slightly lower slope than experiment and again the densities are lower ($< 5\%$). For comparison we have also plotted the density values used in the EAM study by Alemany *et al.* (the open symbols with crosses in Fig. 5). Recall these authors used an experimental value in their simulations. Clearly the value chosen for Cu agrees with the data quoted in Ref. [29] whereas for Ni the density employed in Alemany *et al.*'s study was somewhat lower than the Smithells compilation.

3.2. Solid–liquid interface velocity

In this section the solid–liquid interface velocity as a function of undercooling is reported for three

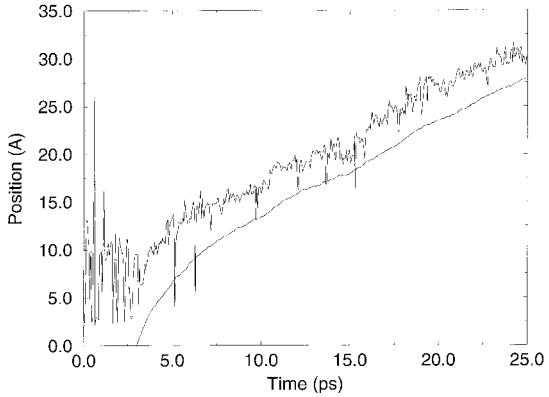

Fig. 6. The position of the solid–liquid boundary as a function of time for Ni at 1500 K. The top corresponds to the intensity method of locating the interface and the bottom curve refers to the total enthalpy method of interface tracking (see text for details).

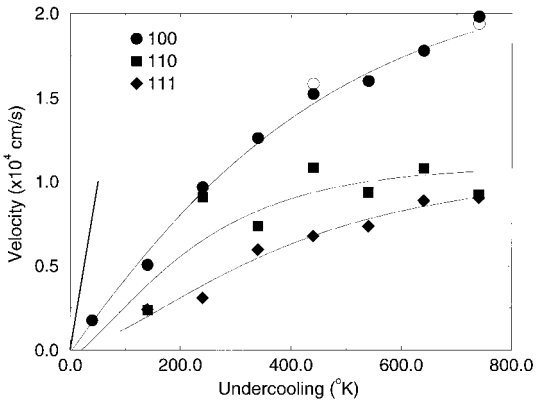

Fig. 7. Boundary velocity as a function of undercooling for Ni in the 100 (circles), 110 (squares) and 111 (diamonds) directions. The thick solid line represents the theoretical upper limit of the velocity as derived by Coriell and Turnbull [30] and the dashed curve is experimental results for Ni [31]. The open circles were computed using an alternate means of MD temperature control.

low index crystal directions: 100, 110 and 111. Molecular dynamics simulations using EAM potentials have been utilized in the past to monitor the motion of a solid phase into the liquid. Foiles and Adams [17] used the vanishing of the interface velocity to approximately determine the melting point of various transition metals and thereby confirmed the melting temperature determined by a Monte-Carlo thermodynamic integration technique. The Adams and Foiles study however did not report values of the interface velocity.

When determining the solid–liquid interface velocity from atomistic simulations, some thought must be given to the method by which the interface position is defined. In the present investigation two techniques were attempted and compared. In the first method the cell is divided into several slices along its length where the slice width is on the order of the lattice parameter and within each slice the intensity of an *in plane* Bragg diffraction peak is computed. For example, for motion of the 100 interface one can define

$$I_{10} = \sum_i \sum_j \cos\left\{ \frac{2\sqrt{2}\pi}{a} [(y_i - y_j) + (z_i - z_j)] \right\} \quad (4)$$

where the y- and z-directions lie normal to the growth direction, a is the lattice parameter and the sum is over all atoms within a given plane. The intensity is very large in the crystal region of the cell and drops very rapidly to near zero in the liquid. The position of the interface can be found by the minimum of the numerical derivative of the intensity vs distance along the cell length.

The second method of obtaining the interface position is through the total enthalpy of the solid–liquid system. At any point in time the total enthalpy is simply the sum of the enthalpy of each phase times the volume fraction of that phase. In other words one can write the interface position, χ, as a function of time:

$$\chi(t) = \frac{X[H_T(t) - H_L]}{2(H_S - H_L)} \quad (5)$$

where the subscripts T, S and L denote total, solid and liquid enthalpies and X is the total length of the cell. The factor of 2 in equation (5) arises from the fact that there are two solid–liquid interfaces moving within the periodic simulation cell.

That the two methods described above yield equivalent interface velocities is demonstrated in Fig. 6. Here the position vs time for Ni at 1500 K ($\Delta T = 240$) is shown, the top curve is the result of the intensity method and the bottom curve represents the enthalpy calculation. The simulation cell is adjusting its temperature and volume over a transient period during which the top curve is rapidly oscillating and the bottom curve is increasing quickly from a large negative value. However, after approximately 0.2 ps the two results predict the same slope, the two curves do not fall exactly on top of one another due to the excess enthalpy associated with the solid–liquid boundary which is not included in equation (5). In the results to follow the enthalpy tracking method was used. Despite the fact that separate calculations are needed at each temperature to obtain the H_S and H_L terms in equation (5), the method is more efficient. Furthermore, as shown in Fig. 6, the enthalpy computation exhibits a much smoother position vs time behavior.

According to Wheeler *et al.* the mobility parameter which governs the kinetics of the phase field evolution can be found from a knowledge of the kinetic coefficient, μ, which relates the velocity of the moving boundary to the undercooling:

$$V = \mu \Delta T = \mu(T_M - T) \quad (6)$$

where T_M is the melting temperature. Equation (6) remains valid in the regime of low undercooling. The velocity vs undercooling behavior required to

obtain μ is shown in Fig. 7 for the case of Ni where the circles denote motion of the 100 face, the squares refer to 110 and the diamonds are the data for the 111 direction. After about $\Delta T = 300$ the linear velocity–undercooling relationship begins to break down and the velocity eventually levels off at very large undercoolings. This general behavior suggested a fit to the simulation data of the form:

$$V = \sum_n a_n \exp(-\alpha n \Delta T). \tag{7}$$

The best fits (with $n = 3$) are shown by the solid lines in Fig. 7 and the values of μ obtained from the limiting behavior as $\Delta T \longrightarrow 0$ and equation (7) are listed in Table 1. An anisotropy of the boundary velocity is found such that $V_{100} > V_{110} > V_{111}$ and there is approximately a factor of two difference in the kinetic constant of the 100 and 111 faces. The thick solid line in Fig. 6 shows the velocity behavior assuming a value of μ equal to 200 cm/s/K. This value of the kinetic coefficient was that used in the aforementioned work of Wheeler *et al.* and represents the theoretical upper limit to the interface velocity. Coriell and Turnbull [30] first established the limiting velocity which is given by

$$\mu = \frac{V_s L}{N k_B T_M} \tag{8}$$

where L is the latent heat of fusion, N is Avogadro's number, k_B is Boltzmann's constant and V_s is the speed of sound in the liquid metal, assumed to be 3×10^5 cm/s. Figure 7 suggests that the actual velocity of the solid–liquid interface in Ni is on the order of a factor of five less than the maximum value.

In a constant temperature MD simulation, coupling to a heat bath is achieved by adding to the equations of motion a drag coefficient times the velocity of the atoms. In the present calculations the drag term is proportional to the difference in actual temperature minus the desired temperature. There are however, alternative schemes of temperature control. For example the method due to Hoover [31] assumes that the derivative of the drag coefficient with respect to time is proportional to the actual and desired temperature difference. It is of interest to check whether the form of temperature control affects the computation of the interface velocity. In Fig. 7 the two open circles at undercoolings of 440 and 740 represent the Hoover control results for the 100 direction of motion. Clearly, within the uncertainty of the velocity measurement the results are independent of the specific MD method of temperature constraint.

Table 1. The kinetic coefficient, μ, for Cu and Ni as a function of growth direction. Also listed are the maximum values predicted theoretically [30]

	hkl	μ (cm/s/K)	Ref. [13]
Ni	100	45	200
Ni	110	32	
Ni	111	18	
Cu	100	46	247
Cu	110	27	
Cu	111	19	

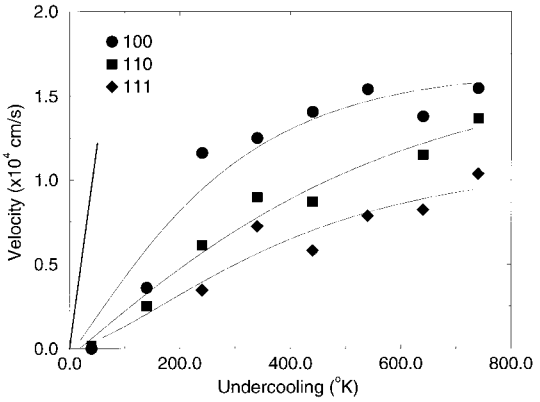

Fig. 8. The interface velocity vs undercooling for pure Cu in the low index 100, 110 and 111 directions. The thick solid line is the theoretical upper limit [30].

Figure 8 shows the velocity vs undercooling behavior for pure Cu where the symbols and lines have the same meaning as in Fig. 7. The solid line corresponds to $\mu = 247$ cm/s/K and again represents the Coriell and Turnbull theoretical upper limit. The ordering of the velocities for Cu is the same as that for Ni, i.e. $V_{100} > V_{110} > V_{111}$, and in fact, as shown in Table 1, the kinetics of interface motion for Cu are very similar to Ni. The similarities of the two elements can perhaps be understood as follows. According to Turnbull and Bagley [32] the velocity of crystal growth depends on the Gibbs free energy difference between the solid and liquid at a given undercooling, the rate at which atoms can jump from the liquid to the solid and the fraction of sites on the interface where growth can occur (i.e. terrace sites). The latter quantity is in turn proportional to the interfacial energy of the crystal face. From the EAM study by Foiles and Adams [17] it is known that the free energy difference vs temperature differs by less than 10% for Cu and Ni. If we assume that the attachment rate is proportional to the diffusion coefficient, then from the previous section it can be seen that at the melting point Ni has a greater diffusivity by about 15%. On the other hand, although the solid–liquid interfacial free energies are not known, Daw *et al.* report [15] that the 100, 110 and 111 excess surface enthalpies for Ni are greater than those of Cu by a similar amount (approximately 20%). Therefore, the similar kinetic behavior observed for Cu and Ni may be a result of offsetting contributions to the growth rate formulation.

Table 1 summarizes the main result of this section. A key point to recognize with regard to phase field modeling is the fact that the interface velocities are a factor of 4–5 less than the theoretical limit. The anisotropy of the 100 and 110 kinetic coeffi-

cient observed for both Cu and Ni can be explained if we make the simplifying assumption that the atomic attachment rate is independent of crystallographic orientation. Under this assumption the velocity for the different directions would simply be related to the different planar spacings. Such a picture holds reasonably well for the 100 and 110 directions. For example the ratio for Ni of μ_{100}/μ_{110} is equal to 1.4 which is the same as the planar spacing ratio of $\sqrt{2}$. On the other hand, μ_{100}/μ_{111} is found to be 2.5 which is 50% higher than $\sqrt{3}$, suggesting the attachment kinetics are somewhat different for the closest packed 111 planes.

4. CONCLUSIONS

In the phase field model of binary solidification two mobility terms appear. One appears in the equation governing the kinetics of the concentration field and the second appears in the equation of motion of the phase field itself. Both of these kinetic terms are difficult to obtain experimentally and as a result the phase field model has only infrequently been used to model real alloy systems. We have presented a means of obtaining the unknown parameters by computing the liquid diffusion coefficient and the solid–liquid interface velocity using MD simulations and EAM potentials.

Molecular dynamics simulations have shown that the diffusivity of both liquid Cu and Ni depends linearly with temperature in the vicinity of the melting point and can be represented by: $D_{\mathrm{Ni}} = 6.92 \times 10^{-4}\Delta T + 0.382$ and $D_{\mathrm{Cu}} = 7.219 \times 10^{-4}(T - T_{\mathrm{M}}) + 0.332$ (10^{-4} cm^2/s). The result for Cu is in good agreement with experiment. The kinetic coefficient relating the solid–liquid boundary velocity to the undercooling was found to vary in the range 45–18 cm/s/K for both Ni and Cu and the anisotropy was such that $\mu_{100} > \mu_{110} > \mu_{111}$. The maximum value of μ was found to be a factor of 4–5 less than the theoretical upper limit.

Acknowledgements—The authors wish to thank A. Karma for many useful discussions. This research was supported by a Sandia Laboratory Directed Research and Development (LDRD) grant and by the U.S. Department of Energy, Office of Basic Energy Sciences, Materials Science Division, under contract number DE-AC04-94AL85000.

REFERENCES

1. Caginalp, G., *Phys. Rev. A*, 1989, **39**, 887.
2. Caginalp, G. and Xie, W., *Phys. Rev. E*, 1993, **48**, 1897.
3. Karma, A. and Rappel, W.J., *Phys. Rev. E*, 1996, **53**, 3017.
4. Karma, A., *Phys. Rev. Lett*., 1993, **70**, 3439.
5. Roy, A., Rickman, J.M., Gunton, J.D. and Elder, K.R., *Phys. Rev. E*, 1998, **57**, 2610.
6. Leo, P.H., Lowengrub, J.S. and Jou, H.J., *Acta mater*., 1998, **46**, 2113.
7. Poduri, R. and Chen, L.Q., *Acta mater*., 1997, **45**, 245.
8. Fan, D. and Chen, L.Q., *Acta mater*., 1997, **45**, 611.
9. Fan, D., Geng, C. and Chen, L.Q., *Acta mater*., 1997, **45**, 1115.
10. Calginalp, G. and Socolovsky, E., *Appl. Math. Lett*., 1989, **2**, 117.
11. Calginalp, G. and Socolovsky, E., *SIAM J. Sci. Comput*., 1991, **15**, 106.
12. Provatas, N., Goldenfeld, N. and Datzig, J., *Phys. Rev. Lett*., 1998, **80**, 3308.
13. Wheeler, A.A., Boettinger, W.J. and McFadden, G.B., *Phys. Rev. A*, 1992, **45**, 7424.
14. Warren, J.A. and Boettinger, W.J., *Acta metall. mater*., 1995, **43**, 689.
15. Daw, M.S., Foiles, S.M. and Baskes, M.I., *Mater. Sci. Rep*., 1993, **9**, 251.
16. Foiles, S.M., *Phys. Rev. B*, 1985, **32**, 3409.
17. Foiles, S.M. and Adams, J.B., *Phys. Rev. B*, 1989, **40**, 5909.
18. Alemany, M.M.G., Rey, C. and Gallego, L.J., *Phys. Rev. B*, 1998, **58**, 685.
19. Alemany, M.M.G., Rey, C. and Gallego, L.J., *J. chem. Phys*, 1998, **109**, 5175.
20. Asta, M., Morgan, D., Hoyt, J. J., Sadigh, B., Althoff, J. D., de Fontaine, D. and Foiles, S. M., *Phys. Rev. B*, 1999, **59**, 14271.
21. Rodriguez de la Fuente, O. and Soler, J.M., *Phys. Rev. Lett*., 1998, **81**, 3159.
22. Foiles, S.M., Baskes, M.I. and Daw, M.S., *Phys. Rev. B*, 1986, **33**, 7983.
23. Voter, A.F. and Chen, S.P., *Mater. Res. Soc. Symp. Proc*., 1987, **82**, 175.
24. Pasquarello, A., Laasonen, K., Car, R., Lee, C. and Vanderbilt, D., *Phys. Rev. Lett*., 1992, **69**, 1982.
25. Allen, M. P. and Tildesley, D. J., *Computer Simulation of Liquids*. Clarendon Press, Oxford, 1987.
26. Hansen, J. P. and McDonald, I. R., *Theory of Simple Liquids*. Academic Press, London, 1976.
27. Reynik, R.J., *Appl. Phys. Lett*., 1966, **9**, 239.
28. Henderson, J. and Yang, L., *Trans. Am. Inst. Min. Engrs*, 1961, **221**, 72.
29. Brandes, E. A. (ed.), *Smithells Metals Reference Book*. Butterworths, London, 1983.
30. Coriell, S.R. and Turnbull, D., *Acta metall*., 1982, **30**, 2135.
31. Hoover, W. G., *Computational Statistical Mechanics*. Elsevier, New York, 1991.
32. Turnbull, D. and Bagley, B. G., *Treatise on Solid State Chemistry*, Vol. 5, N. B. Hannay (ed.). Plenum Press, 1975, p. 513.